

Impact of PET/CT system, reconstruction protocol, data analysis method, and repositioning on PET/CT precision: An experimental evaluation using an oncology and brain phantom

Syahir Mansor*

Department of Radiology & Nuclear Medicine, VU University Medical Center, De Boelelaan 1117, 1081 HV Amsterdam, The Netherlands

Elisabeth Pfaehler*

Faculty of Medical Sciences, Nuclear Medicine and Molecular Imaging, Hanzeplein 1, 9713 GZ Groningen, The Netherlands

Dennis Heijtel

Department of Radiology & Nuclear Medicine, VU University Medical Center, De Boelelaan 1117, 1081 HV Amsterdam, The Netherlands

Martin A. Lodge

PET Center, Johns Hopkins Hospital, Nelson B1125, 1800 Orleans Street, Baltimore, MD 21287, USA

Ronald Boellaard

Department of Radiology & Nuclear Medicine, VU University Medical Center, De Boelelaan 1117, 1081 HV Amsterdam, The Netherlands

Faculty of Medical Sciences, Nuclear Medicine and Molecular Imaging, Hanzeplein 1, 9713 GZ Groningen, The Netherlands

Maqsood Yaqub^{a)}

Department of Radiology & Nuclear Medicine, VU University Medical Center, De Boelelaan 1117, 1081 HV Amsterdam, The Netherlands

(Received 5 March 2017; revised 3 October 2017; accepted for publication 3 October 2017; published 19 November 2017)

Purpose: In longitudinal oncological and brain PET/CT studies, it is important to understand the repeatability of quantitative PET metrics in order to assess change in tracer uptake. The present studies were performed in order to assess precision as function of PET/CT system, reconstruction protocol, analysis method, scan duration (or image noise), and repositioning in the field of view.

Methods: Multiple (repeated) scans have been performed using a NEMA image quality (IQ) phantom and a 3D Hoffman brain phantom filled with ^{18}F solutions on two systems. Studies were performed with and without randomly (< 2 cm) repositioning the phantom and all scans (12 replicates for IQ phantom and 10 replicates for Hoffman brain phantom) were performed at equal count statistics. For the NEMA IQ phantom, we studied the recovery coefficients (RC) of the maximum (SUV_{max}), peak (SUV_{peak}), and mean (SUV_{mean}) uptake in each sphere as a function of experimental conditions (noise level, reconstruction settings, and phantom repositioning). For the 3D Hoffman phantom, the mean activity concentration was determined within several volumes of interest and activity recovery and its precision was studied as function of experimental conditions.

Results: The impact of phantom repositioning on RC precision was mainly seen on the Philips Ingenuity PET/CT, especially in the case of smaller spheres (< 17 mm diameter, $P < 0.05$). This effect was much smaller for the Siemens Biograph system. When exploring SUV_{max} , SUV_{peak} , or SUV_{mean} of the spheres in the NEMA IQ phantom, it was observed that precision depended on phantom repositioning, reconstruction algorithm, and scan duration, with SUV_{max} being most and SUV_{peak} least sensitive to phantom repositioning. For the brain phantom, regional averaged SUVs were only minimally affected by phantom repositioning (< 2 cm).

Conclusion: The precision of quantitative PET metrics depends on the combination of reconstruction protocol, data analysis methods and scan duration (scan statistics). Moreover, precision was also affected by phantom repositioning but its impact depended on the data analysis method in combination with the reconstructed voxel size (tissue fraction effect). This study suggests that for oncological PET studies the use of SUV_{peak} may be preferred over SUV_{max} because SUV_{peak} is less sensitive to patient repositioning/tumor sampling. © 2017 The Authors. *Medical Physics* published by Wiley Periodicals, Inc. on behalf of American Association of Physicists in Medicine. [https://doi.org/10.1002/mp.12623]

Key words: 3D Hoffman brain phantom, IQ NEMA phantom, PET/CT, phantom repositioning, repeatability, reproducibility

1. INTRODUCTION

[^{18}F]Fluorodeoxyglucose (^{18}F -FDG) positron emission tomography and computed tomography (PET/CT) is being used for staging and tumor response assessment in oncology.^{1–7} The analysis of [^{18}F]-FDG uptake in tumors can be performed semiquantitatively using the standard uptake value (SUV) rather than using visual assessment of relative change. The main drawback of using SUV is its sensitivity to various technical factors, such as image reconstruction settings⁹ and segmentation strategies.^{10–12} The impact of different image acquisition and processing methods on SUV are well understood and to mitigate these effects,¹³ various standardization efforts are made, especially in multicenter clinical trials. In order to yield a high reproducibility, standard operating procedures (SOPs) or guidelines need to be followed that address patient preparation, image acquisition and processing, and data analysis and interpretation. For longitudinal studies, i.e., when quantitatively measuring tumor response to therapy, it is important to understand the precision of the quantitative metric being used to measure change in tracer uptake. Several studies have reported^{14–16} repeatabilities ranging from 10% to 15%, on average. This precision arises from several clinical and technical contributions, such as uncertainties in administered activity, variability in patient preparation and physiological condition (blood glucose level) *et cetera*, and also from image noise due to variability in scan statistics. Very few FDG SUV precision studies report within-patient coefficients of variation less than 10% and it is unclear if this is limited by technical as opposed to patient-related factors. Technical limitations have partly been assessed using phantoms filled with long half-life isotopes and reassessed at multiple PET centers.¹⁷ However, these effects were not yet assessed for brain protocols using an anthropomorphic brain phantom. In addition, new reconstruction algorithms have been developed for clinical PET/CT systems, incorporating the system point spread function, that are able to improve spatial resolution.

The aim of this study was, therefore, to experimentally evaluate PET/CT precision dependence on reconstruction protocol, scan duration, and image analysis methods. Most importantly we compared to what extent precision of various quantitative uptake metrics obtained with different reconstruction protocols, voxel sizes, and scan durations depend on phantom repositioning versus static placement of the phantom. These studies were performed for both an oncology and brain phantom. In most experimental studies reported to date the repositioning aspect was not included. As partial volume effects are in part caused by the so-called tissue fraction effect (voxel size), the actual ‘voxel sampling’ of small objects may be an additional source of uncertainty. In clinical longitudinal studies, patients are not repositioned in exactly the same manner during all scans. Therefore, it is important to assess these repositioning effects and to determine which of the analysis methods can mitigate these effects best. To this end, PET phantoms for quantitative performance assessment were scanned on two different PET/CT systems. The acquisitions were repeated ($n = 12$ for IQ phantom and

$n = 10$ for Hoffman brain phantom) with and without phantom repositioning, while keeping count statistics equivalent between replicates. Additionally, the acquired data were reconstructed using various clinically applied reconstruction protocols and frame durations. All data were analyzed with common quantitative metrics, such as SUV_{max} , SUV_{peak} , or SUV_{mean} .

2. MATERIALS AND METHODS

2.A. Phantom experiments

Phantom experiments were performed on an Ingenuity PET/CT scanner (Philips Healthcare, Cleveland, OH, USA) and the Biograph mCT 40 (Siemens Healthcare, Knoxville, TN, USA). All emission data were reconstructed using the vendor-provided time of flight iterative reconstruction method including all corrections needed for quantification such as scatter, random, normalization, and attenuation correction. The Philips Ingenuity system uses an iterative reconstruction algorithm (BLOB-OS-TF) with 3 iterations and 33 subsets, and the Siemens Biograph system uses a 3D iterative reconstruction algorithm (OSEM) with 3 iterations and 21 subsets. For both systems, a low-dose CT, using vendor recommended settings, was used for attenuation correction.

Moreover images were generated with and without point spread function (PSF) or resolution modeling. For the Philips Ingenuity PET/CT system, the resolution modeling is implemented as a postreconstruction iterative deconvolution method (and used with the vendor provided default settings). The Philips Ingenuity system reconstructs images with a voxel size of either $4 \times 4 \times 4 \text{ mm}^3$ or $2 \times 2 \times 2 \text{ mm}^3$ with a corresponding matrix of $144 \times 144 \times 45$ or $288 \times 288 \times 90$ for body mode acquisitions. Brain mode acquisitions yield images with a voxel size of $2 \times 2 \times 2 \text{ mm}^3$ and a matrix of $128 \times 128 \times 90$ (applied only in case of the 3D Hoffman phantom, as discussed below). Resolution modeling on the Siemens Biograph system is implemented within the reconstruction process, i.e., included in the system matrix. Data collected on the Siemens Biograph PET/CT system are reconstructed with a voxel size of either $3.1819 \times 3.1819 \times 2 \text{ mm}^3$ or $2.0364 \times 2.0364 \times 2 \text{ mm}^3$ with a corresponding matrix of $256 \times 256 \times 111$ or $400 \times 400 \times 111$ for body mode acquisitions. Brain mode acquisitions are reconstructed with a voxel size of $2.0364 \times 2.0364 \times 2 \text{ mm}^3$ and matrix of $400 \times 400 \times 111$.

Two different phantoms were evaluated. First, the NEMA NU-2 Image Quality (IQ) phantom (Data Spectrum, Hillsborough, NC, USA) was used. This phantom is well known for its use in NEMA NU-2 IQ PET performance measurements and for its use in standardization of multicenter PET studies (EANM-EARL).¹⁸ The phantom consists of a large background volume (9400 mL) with six spheres with inner diameters of 10, 13, 17, 22, 28, and 37 mm. The spheres and the background were filled with an ^{18}F solution following EANM/EARL recommendations and resulted in sphere/background ratios of approximately 10:1. The ‘true’ activity

concentration in the phantom was derived from the activity measurement with a dose-calibrator and the known volume of the phantoms. Moreover, activity concentrations were cross-checked by measuring samples on a gamma well counter. Two series of scans were performed for each PET/CT system. First, the IQ phantom was filled once (ranging from 1.75 to 3.08 kBq ml⁻¹ in the background compartment and 17.78 to 28.63 kBq ml⁻¹ in the spheres) and scanned in one fixed position for 120 min. Data were reconstructed in 12 frames at three different frame durations (2, 4, and 5 min for the first reconstructed frame). In order to keep scan statistics constant between all reconstructed images, frame duration was increased for each subsequent reconstructed frame to compensate for radioactive decay (i.e., yielding similar count statistics for each subsequent frame). Secondly, the IQ phantom was filled once and rescanned (both low-dose CT and PET) 12 times while randomly repositioning the phantom at different angles along any axis (< 5 degrees) and translations (x, y, z), resulting in displacements of up to 20 mm. Each of the acquisitions was reconstructed with frame durations to yield the same count statistics as achieved with the first set of (stationary phantom) measurements.

Secondly, we acquired data for the 3D Hoffman brain phantom (Data Spectrum, Hillsborough, NC, USA). Similar to the IQ phantom experiment, the phantom was scanned in two series for each PET/CT system: one using the same phantom position over 120 min (activities ranging from 59.69 to 125 MBq in the phantom at start scanning) and a series consisting of rescanning at 10 different phantom repositions (activities ranging from 62.34 to 114 MBq in the phantom at start scanning). Similar to the IQ phantom studies, data were reconstructed with three different frame durations (2, 4, and 5 min for the first frame). The frame duration was again increased to compensate for radioactive decay (i.e., yielding similar count statistics for each frame).

2.B. Regional assessments

Regional assessment of the experiments was performed using several automated (IQ Phantom) and manual image segmentation methods (3D Hoffman phantom). Automated segmentation of the spheres of the IQ phantom was performed using the EARL analysis tool which generated volumes with background corrected isocontours set at 50% of SUV_{max}.¹⁸ From these delineations, we derived the maximum (SUV_{max}), peak (SUV_{peak}), and mean (SUV_{mean}) uptake in each of the images. The peak SUV was derived from a 1 ml spherical volume of interest (VOI) positioned to yield the highest average VOI value across the lesion (or sphere in case of the phantom). Note that the VOI analysis was performed on the original images without image registration to resemble clinical conditions as closely as possible. Next, we derived the recovery coefficient (RC_{max}, RC_{peak}, and RC_{mean}) by dividing observed max, peak, and mean values by the expected activity concentrations. RCs were derived for each sphere and for all acquired and reconstructed emission images. RCs precision as a function of sphere size, data

analysis method (max, peak, and mean), and reconstruction methods for both stationary and repositioning phantom experiments was evaluated.

For the 3D Hoffman brain phantom, several volumes of interest (VOIs) were drawn manually using a coregistered binary mask of gray and white matter of the phantom. For each hemisphere in total, five different VOIs for gray and five VOIs for white matter of different sizes were drawn as shown in Fig. 1. VOI were chosen to obtain activity concentration estimates for both cortical and more deeply located brain structures. From these VOIs, we derived the mean regional activity concentration and compared these with the actual activity concentration of the solution used to fill the phantom to produce the RC_{mean}. For the repositioned phantom study, this VOI template was rigidly realigned onto the original phantom images.

3. RESULTS

3.A. NEMA IQ phantom

Figures 2 and 3 illustrate recovery coefficients for the IQ phantom for images with 5-min scan duration. In general, repositioning of the phantom increased variability of RC data compared with the stationary phantom data especially for the Philips Ingenuity system (Table I). The additional variability due to repositioning was larger when using RC_{max} and/or using reconstructions that include PSF. Also, for both systems, use of TOF + PSF produced higher recoveries than TOF reconstruction alone and this effect (> 5% increase) was largest for RC_{max} observed with the Siemens Biograph system [Fig. 3(b)]. The PSF implementation on the Siemens Biograph also affects the smaller spheres more as compared to the implementation on the Philips Ingenuity system, which resulted in an increased RC and also strongly increased variability [Figs. 2(b), 2(f), 3(b) and 3(f)]. In supporting information Figs. S1 and S2, recovery coefficients observed for the IQ phantom for images with 2-min scan duration are shown. Although these RCs showed somewhat larger variability, as expected due to the lower count statistics as compared to 5-min data, overall trends were similar to those of the 5-min data.

Recovery coefficients for images reconstructed with smaller voxel sizes (2 × 2 × 2 mm³) are shown in Figs. 4 and 5 (5-min scan duration) and supporting information Figs. S3 and S4 (2-min scan duration). Comparing the differences between Fig. 2 and 4 and between Fig. 3 and 5 showed that smaller voxel sizes result in increased variability in the observed recoveries. This effect is larger for the Philips Ingenuity than for the Siemens Biograph system. For both scanners, the variability of RC was now comparable between repositioning and stationary phantom experiments (Table II). Moreover, shorter frame durations increased variability in the observed recoveries. In general, RC_{max} was more sensitive to noise and phantom repositioning than the other quantitative metrics. Tables I and II summarize the *F*-test significance (not corrected for multiple comparisons), for differences in

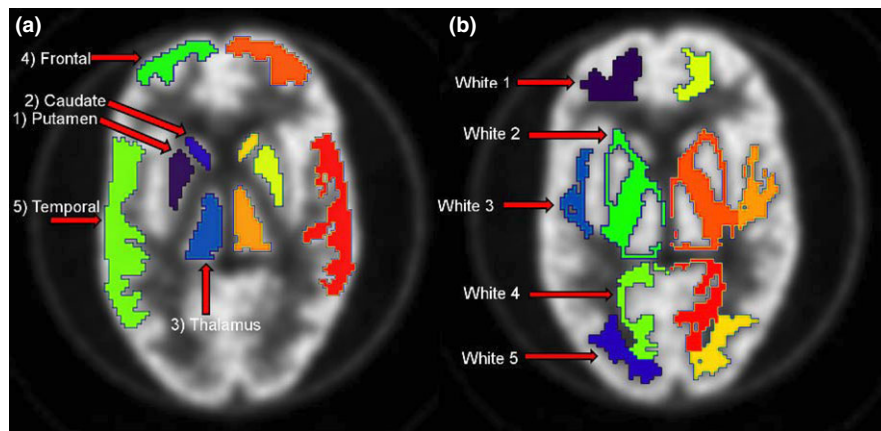


FIG. 1. Illustration of VOIs in gray matter for both brain hemispheres in (A) and VOIs in white matter in (B). These VOIs were used to assess RC for different brain structures and regions as function of experimental condition. [Color figure can be viewed at wileyonlinelibrary.com]

precision between the stationary scan and repositioning phantom data for the various analysis methods and voxel sizes.

3.B. 3D Hoffman brain phantom evaluation

Box plots in Fig. 6 demonstrate the RC_{mean} for several gray matter regions drawn in the Hoffman brain phantom acquired on the Philips Ingenuity system. There was no significant difference in RC variability between repositioned and stationary scans and when using shorter frame durations (data not shown). PSF-based reconstructions yielded slightly higher RCs ($\sim 3\%$). Gray matter recoveries were similar, but slightly more variable for the repositioning data, on the Siemens Biograph system (data not shown). Figure 7 shows RC_{mean} for the white matter regions acquired on the Philips Ingenuity system. For white matter, the Philips Ingenuity system showed $\sim 10\%$ lower values than the Siemens Biograph system. In addition, for the Philips Ingenuity system with PSF reconstruction, the RC values were slightly lower than those obtained without PSF in white matter regions, while the Siemens Biograph system yielded similar results for the reconstructions with and without PSF.

4. DISCUSSION

4.A. NEMA IQ phantom

The impact of phantom repositioning on RC precision can clearly be seen in Figs. 2 and 3 (and supporting information Figs. S1 and S2), especially in the case of smaller spheres (< 17 mm diameter, Table I, $P < 0.05$) for all analysis methods used. However, this effect was smaller for the Siemens Biograph system, possibly because of the smaller voxel sizes in body mode imaging (20.2 mm^3) compared with those used on the Philips Ingenuity system (64.0 mm^3). This finding is supported by reconstructions with smaller voxel sizes for both systems showing that phantom repositioning has a smaller impact on RC precision if smaller voxel sizes ($2 \times 2 \times 2 = 8 \text{ mm}^3$) are used

(Figs. 4 and 5, and supporting information Figs. S3 and S4). Although some of the differences were statistically significant (Tables I and II), the actual differences are very small and likely clinically not relevant. In case of smaller voxels ($< 4 \times 4 \times 4 \sim 64 \text{ mm}^3$), the impact of noise (due to less count per voxel) seems to have a larger effect on RC variability than that resulting from phantom repositioning. The precision is even worse when shorter scan durations are used in combination with small voxel sizes as shown in supplemental Figs. 3 and 4. For all reconstructions, use of regionally averaged values, such as in case of RC_{mean} or RC_{peak} shows less dependence on phantom repositioning than RC_{max} . Moreover, it was found that particularly RC_{max} shows upward bias with decreasing scan duration or worse scan statistics, as was shown before by Boellaard et al.,¹⁰ Lodge et al.,¹⁹ and Doot et al.¹⁷ A possible strategy to reduce uncertainty caused by scanner differences, noise and repositioning could therefore be achieved by the use of SUV_{peak} and this method might be the method of choice for tumor imaging in a clinical setting. Our findings are in good agreement with the study by Lodge et al.¹⁹ suggesting that the peak value is a more robust metric, not only experimentally²⁰ but also in clinical practice.¹⁹ Moreover, as was shown by Makris et al.,²¹ SUV_{peak} depends less on differences in image resolution and might, therefore, be an attractive method in multicentre studies. A drawback of SUV_{peak} is the lower recovery for smaller spheres/tumors when the size of the peak VOI is equal to or larger than that of the sphere/tumor such that background activity is included within the VOI. The latter explains also why for the Siemens data in Fig. 3, when using PSF during the reconstructions, RC_{peak} still show low recoveries for the smallest spheres, while much higher recoveries were seen for RC_{max} or RC_{mean} . The low recoveries of SUV_{peak} for small spheres (< 12 mm diameter) may hamper its application for very small tumors and the use of SUV_{peak} in a longitudinal setting, e.g., to measure treatment response, therefore warrants further exploration.

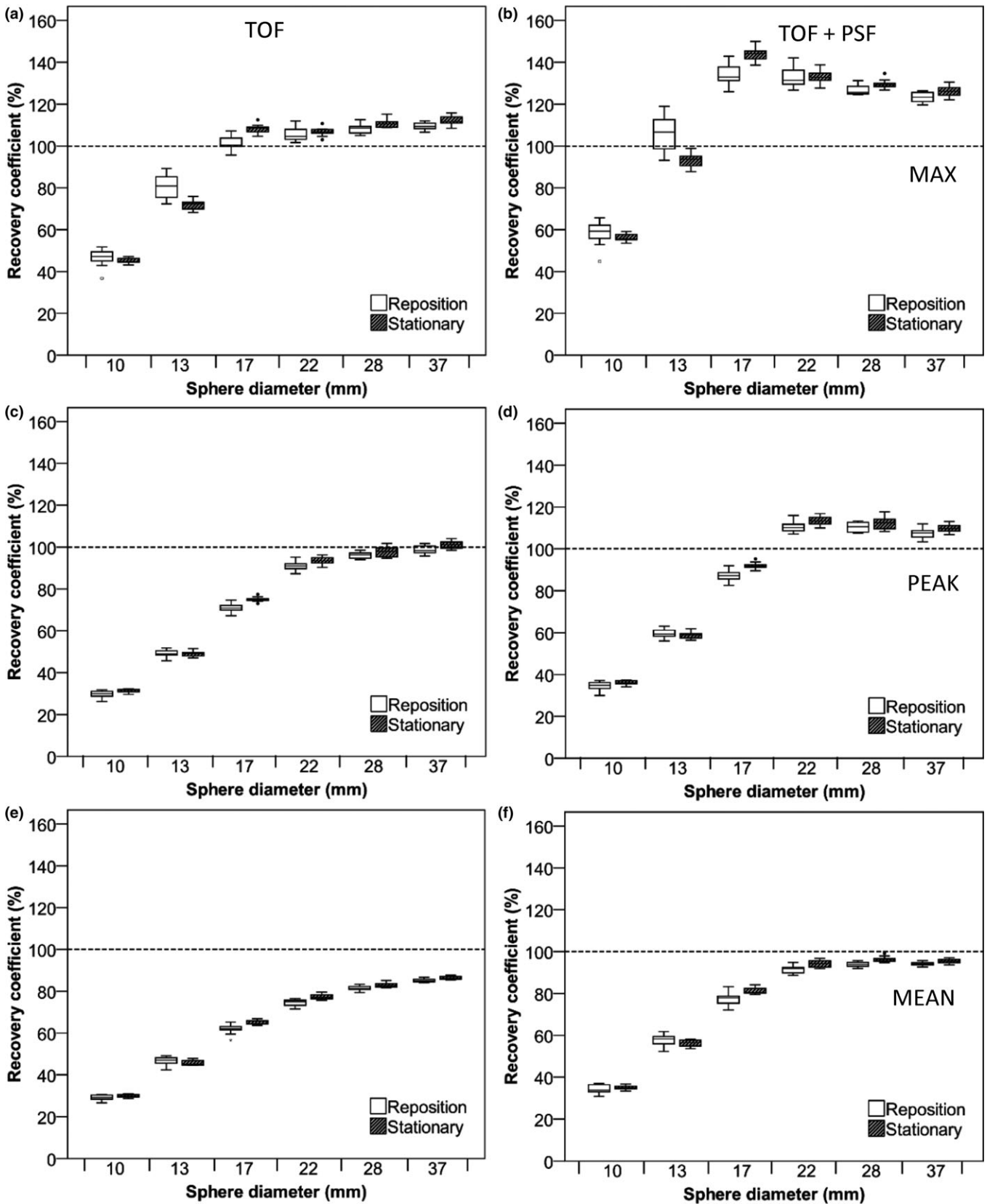


FIG. 2. RC of NEMA IQ phantom data as a function of sphere diameter. Data were acquired on the Philips Ingenuity system and based on images with a $4 \times 4 \times 4 \text{ mm}^3$ voxel size and 5-min starting frame duration using TOF on the left column and TOF + PSF on the right column. Figures (A and B) represent RC (%) for max, (C and D), peak, and (E and F) mean SUVs. Dotted lines correspond to the true RC based on the true activity within the phantom spheres. Boxes represent standard deviation (SD), whiskers show ranges, and solid line depicts median of the data.

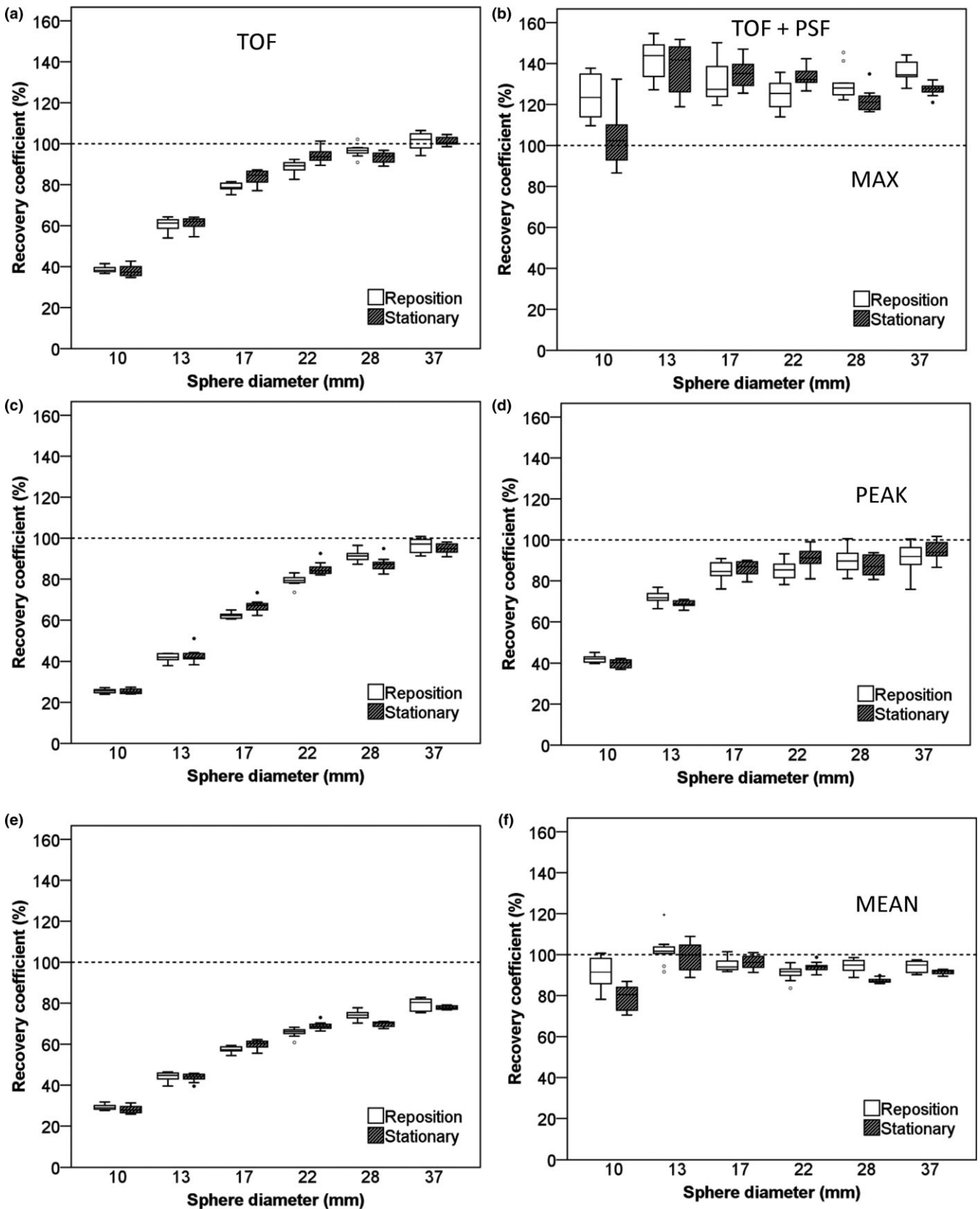


FIG. 3. RC of NEMA IQ phantom data as a function of sphere diameter. Data were acquired on the Siemens Biograph system and based on images with a $3.1819 \times 3.1819 \times 2$ mm voxel size and 5-min starting frame duration using TOF on the left column and TOF + PSF on the right column. Figures (A and B) represent RC (%) for max, (C and D), peak, and (E and F) mean SUVs. Dotted lines correspond to the true RC based on the true activity within the phantom spheres. Boxes represent standard deviation (SD), whiskers show ranges, and solid line depicts median of the data.

TABLE I. Significant P values (not corrected for multiple comparisons) calculated by performing F -tests between repositioned and stationary phantom datasets for different analysis and reconstruction methods and for each sphere and for 5-min scan duration data with $4 \times 4 \times 4 \text{ mm}^3$ voxel sizes for the Philips Ingenuity system and $3.1819 \times 3.1819 \times 2 \text{ mm}^3$ voxel sizes for the Siemens Biograph system. Nonsignificant values are indicated with – for clarity reasons.

	Sphere diameter (mm)	TOF (SUV _{max})	TOF + PSF (SUV _{max})	TOF (SUV _{peak})	TOF + PSF (SUV _{peak})	TOF (SUV _{mean})	TOF + PSF (SUV _{mean})
Philips ingenuity	10	0.001	0.001	0.001	0.010	0.053	0.013
	13	0.002	0.002	–	–	0.036	0.034
	17	0.018	4.5×10^{-8}	0.002	1.2×10^{-8}	0.003	4.08×10^{-8}
	22	–	–	–	–	–	–
	28	–	–	–	–	–	–
	37	–	–	–	–	–	–
Siemens biograph mCT40	10	–	0.001	–	0.006	–	0.01
	13	–	–	–	0.009	–	–
	17	0.001	–	0.001	–	0.003	–
	22	0.001	0.040	0.004	0.030	0.002	0.032
	28	0.013	–	0.003	–	0.001	0.001
	37	–	0.001	–	–	–	–

The choice of acquisition settings and reconstruction algorithm can also heavily affect the quantitative precision. As expected, shorter scans (i.e., 2-min scan duration) tend to provide overestimated RC_{max} which is consistent with the finding by Boellaard et al.¹⁰ and Akamatsu et al.²⁰ Furthermore, data in this study showed an increase in RC variability from 20 to 30% when using reconstructions that include PSF for both repositioned and stationary data. Even in the stationary phantom study, recoveries varied with reconstruction protocol which is in agreement with Armstrong et al.²²

4.B. Hoffman brain phantom

The Hoffman brain phantom consists of a complex structure that mimics the structure of the human brain. The measurement of tracer uptake in small brain structures such as the caudate and putamen can be hampered by partial volume effects. For the Philips Ingenuity system, the inclusion of the PSF in the reconstruction increased gray matter region RC_{mean} up to 5%–10% compared to those seen without PSF. On the other hand, RC_{mean} in white matter regions was reduced by 2%–5% when using PSF. These effects found for the Philips Ingenuity system are consistent with that by Shao et al.²³ The data for the Siemens Biograph system were much less affected by use of PSF in the brain phantom experiment (< 2%), although visually images appear to have a higher resolution. These results can be expected as the use of PSF results in improved spatial resolution and should, therefore, result in higher recoveries in gray matter structures and lower ones for white matter. However, it should be noted that use of PSF may introduce Gibbs artifacts as well, which in turn could lead to activity concentration overestimations.²⁴

Statistical analysis performed on the data from the Philips system showed a significant difference between repositioned and stationary phantom scans for both gray and white matter VOIs. However, the differences were very small (< 5%) and likely not clinically relevant. The low sensitivity of RC

variability for phantom repositioning likely results from the use of regionally averaged values. This was also observed in the NEMA IQ phantom, where SUV_{mean} seems to be less sensitive to phantom (re-)positioning than SUV_{max}. Therefore, spatially averaging data over an extended volume of interest seems to mitigate the effects of phantom repositioning and/or (voxel) sampling of the phantom. Although the distribution of the radiotracer in the Hoffman brain phantom is assumed to be uniform within gray and white matter regions, the distribution in a real human brain might exhibit larger variations. Therefore, it cannot be ruled out that there is an effect of patient repositioning on the precision of regional average values in clinical practice.

4.C. Future perspectives

This study confirms several findings from previous studies, such as precision dependence on scan statistics/duration, data analysis methods and reconstruction protocol, and may therefore be assumed to be generally applicable. In our work, we extended earlier studies by including the effects of repositioning in order to resemble the clinical conditions encountered in longitudinal studies for both oncology body scans as well as brain PET studies. We found that phantom repositioning and thereby tumor voxel sampling variations particularly affected the precision of SUV_{max} analysis for small spheres, while the use of regionally averaged values by SUV_{peak} or SUV_{mean} mitigated these uncertainties (in part). The latter can be understood easily as averaging data over multiple voxels mitigate some of the sampling effect. In particular, use of a fixed size VOI, such as SUV_{peak}, generates uptake values that can be expected to be less influenced by voxel size provided fractional voxel coverage by the SUV_{peak} is taken into account appropriately, as was the case in this study.

A limitation of our work was the use of random repositioning of the phantom rather than applying systematic displacements in axial and transaxial directions. The latter

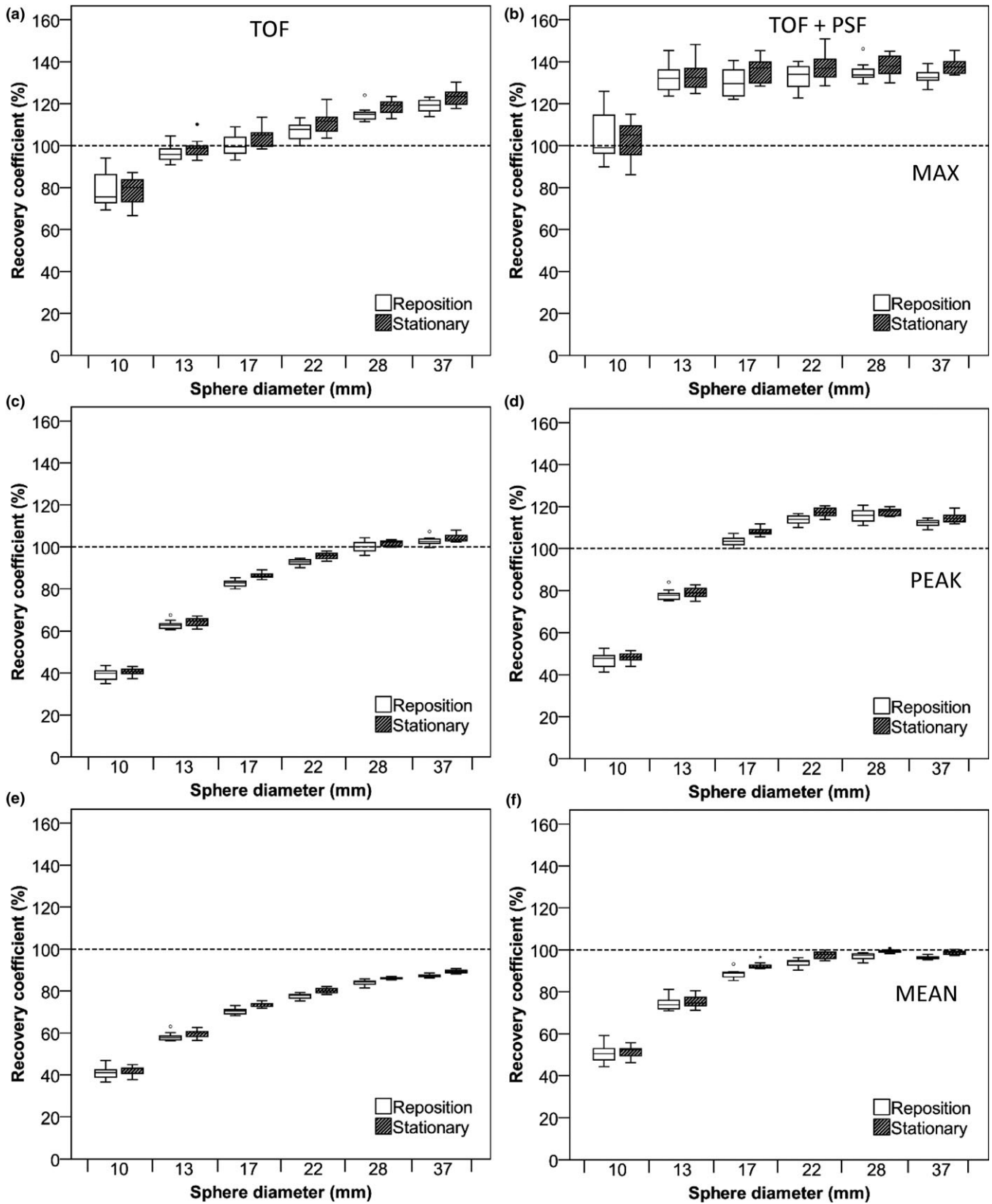


FIG. 4. RC of NEMA IQ phantom data as a function of sphere diameter. Data were acquired on the Philips Ingenuity system and based on images with a $2 \times 2 \times 2 \text{ mm}^3$ voxel size and 5-min starting frame duration using TOF on the left column and TOF + PSF on the right column. Figures (A and B) represent RC (%) for max, (C and D), peak, and (E and F) mean SUVs. Dotted lines correspond to the true RC based on the true activity within the phantom spheres. Boxes represent standard deviation (SD), whiskers show ranges, and solid line depicts median of the data.

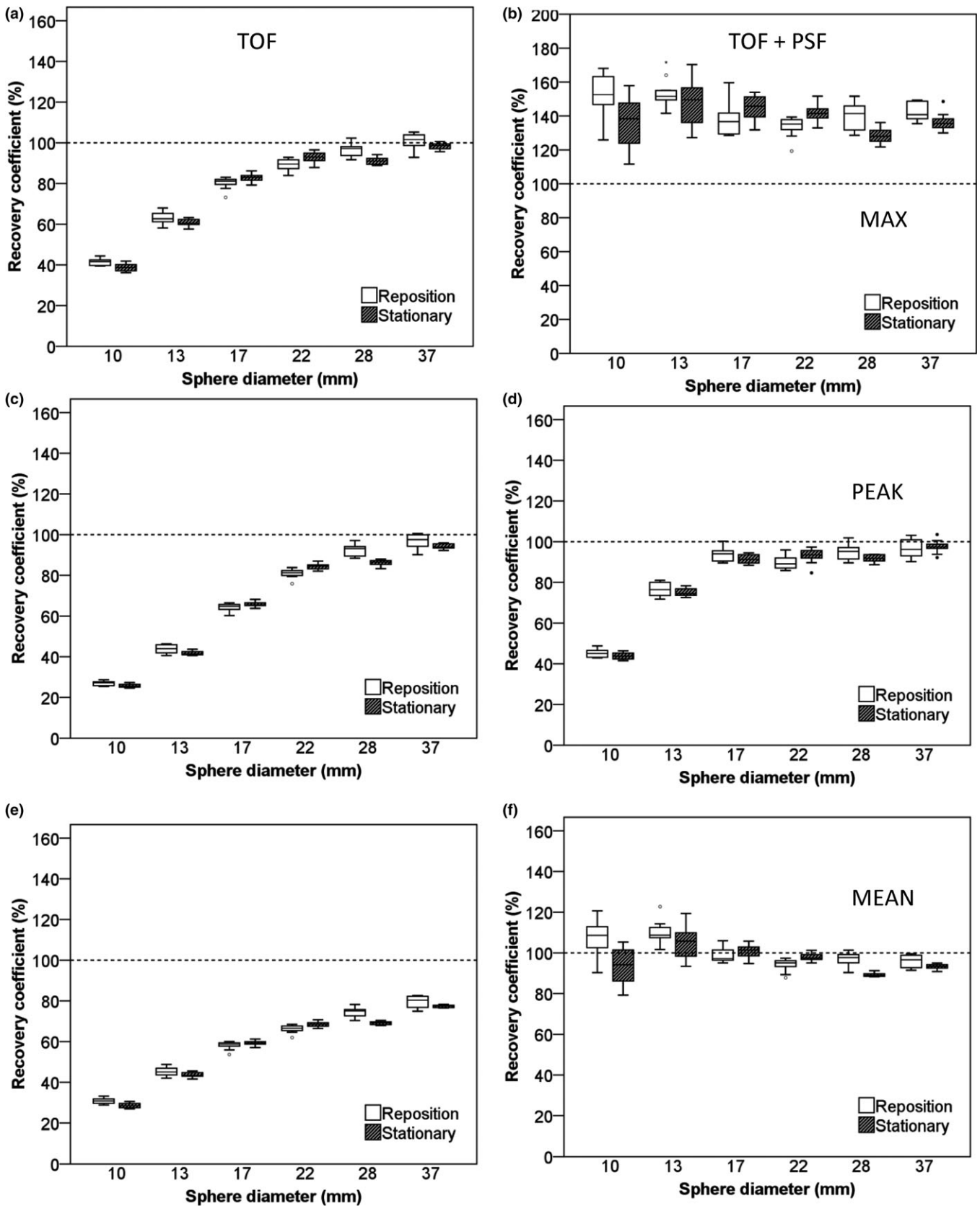


FIG. 5. RC of NEMA IQ phantom data as a function of sphere diameter. Data were acquired on the Siemens Biograph system and based on images with a $2 \times 2 \times 2 \text{ mm}^3$ voxel size and 5-min starting frame duration using TOF on the left column and TOF + PSF on the right column. Figures (A and B) represent RC (%) for max, (C and D) peak, and (E and F) mean SUVs. Dotted lines correspond to the true RC based on the true activity within the phantom spheres. Boxes represent standard deviation (SD), whiskers show ranges, and solid line depicts median of the data.

TABLE II. Significant *P* values (not corrected for multiple comparisons) calculated by performing *F*-tests between repositioned and stationary phantom datasets for different analysis and reconstruction methods and for each sphere and for 5-min scan duration data with $2 \times 2 \times 2 \text{ mm}^3$ voxel sizes for both the Philips Ingenuity system and the Siemens Biograph system. Nonsignificant values are indicated with – for clarity reasons.

	Sphere diameter (mm)	TOF + PSF					
		TOF (SUV _{max})	(SUV _{max})	TOF (SUV _{peak})	TOF + PSF (SUV _{peak})	TOF (SUV _{mean})	TOF + PSF (SUV _{mean})
Philips ingenuity	10	0.006	–	–	–	–	–
	13	0.005	–	–	–	–	–
	17	0.010	–	–	–	–	0.002
	22	0.001	–	–	–	–	–
	28	–	–	0.021	0.028	0.003	0.009
	37	0.016	–	–	–	–	–
Siemens biograph mCT40	10	0.046	0.011	0.025	–	0.032	0.020
	13	–	–	0.008	–	–	–
	17	0.024	–	–	–	–	–
	22	0.001	0.004	0.001	0.027	0.001	0.004
	28	0.007	0.001	0.003	0.047	0.000	0.001
	37	–	0.011	–	–	–	0.021

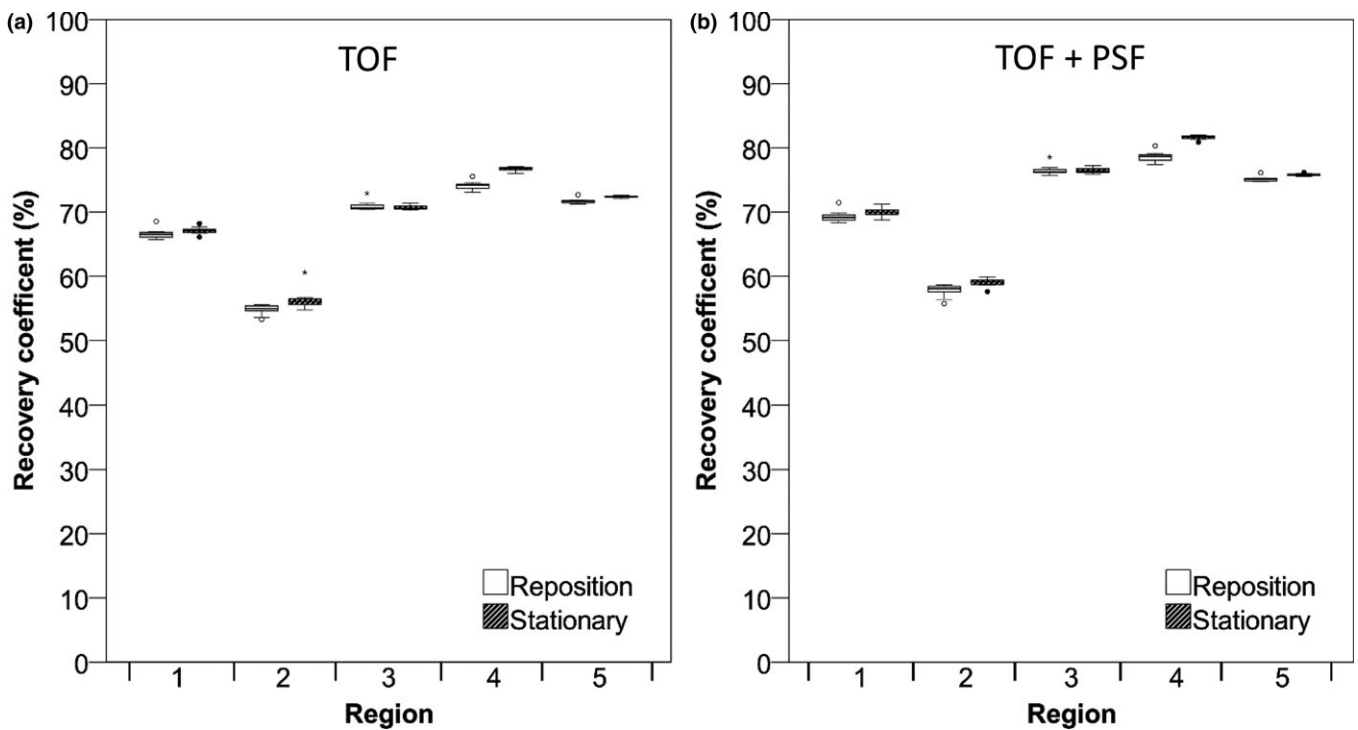


FIG. 6. RC (%) of Hoffman phantom data in different gray matter regions. Data were acquired on the Philips Ingenuity system and reconstructed using TOF (A) and TOF + PSF (B). RC for 5-min frame duration are shown. Boxes represent standard deviation (SD), whiskers show ranges, and solid line depicts median of the data.

would have allowed to determining the effect of axial versus transaxial resolution of the system on the observed precisions. In our study, we have chosen to randomly reposition the phantom to resemble clinical practice and we assumed that use of 12 or 10 replicates would provide sufficient understanding of PET uncertainty dependence on phantom repositioning as our results are in line with previous reports (using non-PSF reconstructions¹⁷).

Secondly, in our paper, we focused only on some technical aspects or factors that could affect PET precision. Yet, there

are many other sources of uncertainty in clinical practice,²⁵ such as net injected activity, patient preparation procedures, uptake time variability, use of different data analysis software, scanner calibration errors, etc. that may have a much larger effect on PET precision than the effect of e.g., repositioning. The observed increased variability of SUV_{max} with IQ phantom repositioning is small compared to the uncertainties resulting from other factors, in particular when PET studies are not strictly performed in compliance with international guidelines. Yet, the authors believe that by using quantitative

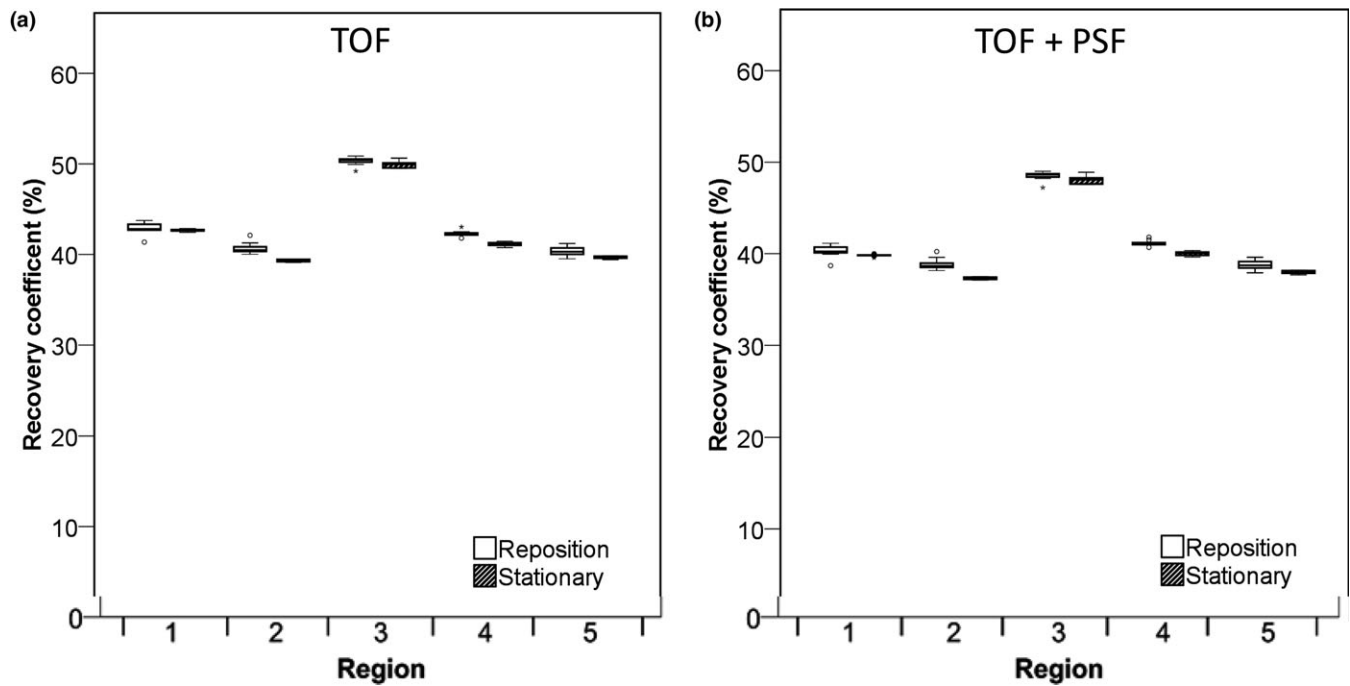


FIG. 7. RC (%) of Hoffman phantom for different white matter regions. Data were acquired on the Philips Ingenuity system and reconstructed using TOF are shown (A) and with TOF + PSF in (B). Data for 5-min frame durations are shown. Boxes represent standard deviation (SD), whiskers show ranges, and solid line depicts median of the data.

metrics, such as SUV_{peak} , that may mitigate even relatively small sources of error could improve the repeatability and reproducibility of quantitative PET reads and are worth further exploration.

5. CONCLUSIONS

Precision of quantitative tracer uptake values depends on scan duration, data analysis methods, reconstruction protocol, and phantom repositioning. The latter effect was most pronounced in an oncological experimental phantom setting for smaller spheres (< 15 mm diameter) when using SUV_{max} . When using either fixed sized VOIs (SUV_{peak} in the IQ phantom) or using regionally averaged data (brain phantom), the impact of phantom repositioning on quantitative precision is minimal. As in longitudinal studies it is impossible to exactly put the patient in the same position in the PET/CT system, it would be preferred to quantify tracer uptake using methods that are insensitive to patient repositioning. The use of SUV_{peak} in an oncological setting may, therefore, be a good alternative to SUV_{max} , but its use for smaller lesions needs to be further studied due to the lower recoveries seen for spheres smaller than 15 mm diameter.

ACKNOWLEDGMENT

Syahir Mansor is a PhD student and was supported by a scholarship from the Malaysian Ministry of Education and University Sains Malaysia. This study was financially supported by the Quantitative Imaging Biomarker Alliance (QIBA) under project NIBIB HHSN268201500021C. This

work is part of the research program STRaTeGy with project number 14929, which is (partly) financed by the Netherlands Organisation for Scientific Research (NWO).

CONFLICT OF INTEREST

None. Dennis Heijtel is currently being employed by Philips Healthcare.

*Both authors contributed equally.

^{a)} Author to whom correspondence should be addressed. Electronic mail: maqsood.yaqub@vumc.nl; Telephone: +31 (0)20 4444346.

REFERENCES

- Dehdashti F, Siegel BA, Griffeth LK, et al. Benign versus malignant intraosseous lesions: discrimination by means of PET with 2-[F-18] fluoro-2-deoxy-D-glucose. *Radiology*. 1996;200:243–247.
- Hoekstra CJ, Hoekstra OS, Stroobants SG, et al. Methods to monitor response to chemotherapy in non-small cell lung cancer with 18F-FDG PET. *J Nucl Med*. 2002;43:1304–1309.
- Hoekstra CJ, Paglianiti I, Hoekstra OS, et al. Monitoring response to therapy in cancer using [18F]-2-fluoro-2-deoxy-D-glucose and positron emission tomography: an overview of different analytical methods. *Eur J Nucl Med*. 2000;27:731–743.
- Krak NC, van der Hoeven JJ, Hoekstra OS, Twisk JW, van der Wall E, Lammertsma AA. Measuring [(18)F]FDG uptake in breast cancer during chemotherapy: comparison of analytical methods. *Eur J Nucl Med Mol Imaging*. 2003;30:674–681.
- Aoki J, Watanabe H, Shinozaki T, et al. FDG-PET for preoperative differential diagnosis between benign and malignant soft tissue masses. *Skeletal Radiol*. 2003;32:133–138.
- Aoki J, Watanabe H, Shinozaki T, et al. FDG PET of primary benign and malignant bone tumors: standardized uptake value in 52 lesions. *Radiology*. 2001;219:774–777.

7. Hubner KF, Buonocore E, Gould HR, et al. Differentiating benign from malignant lung lesions using “quantitative” parameters of FDG PET images. *Clin Nucl Med*. 1996;21:941–949.
8. Wahl RL, Jacene H, Kasamon Y, Lodge MA. From RECIST to PERCIST: evolving considerations for PET response criteria in solid tumors. *J Nucl Med*. 2009;50:122S–150S.
9. Jaskowiak CJ, Bianco JA, Perlman SB, Fine JP. Influence of reconstruction iterations on 18F-FDG PET/CT standardized uptake values. *J Nucl Med*. 2005;46:424–428.
10. Boellaard R, Krak NC, Hoekstra OS, Lammertsma AA. Effects of noise, image resolution, and ROI definition on the accuracy of standard uptake values: a simulation study. *J Nucl Med*. 2004;45:1519–1527.
11. Stahl A, Ott K, Schwaiger M, Weber WA. Comparison of different SUV-based methods for monitoring cytotoxic therapy with FDG PET. *Eur J Nucl Med Mol Imaging*. 2004;31:1471–1478.
12. Krak NC, Boellaard R, Hoekstra OS, Twisk JW, Hoekstra CJ, Lammertsma AA. Effects of ROI definition and reconstruction method on quantitative outcome and applicability in a response monitoring trial. *Eur J Nucl Med Mol Imaging*. 2005;32:294–301.
13. Boellaard R, Delgado-Bolton R, Oyen WJ, et al. FDG PET/CT: EANM procedure guidelines for tumour imaging: version 2.0. *Eur J Nucl Med Mol Imaging*. 2015;42:328–354.
14. Kramer GM, Frings V, Hoetjes N, et al. Repeatability of quantitative whole-body 18F-FDG PET/CT uptake measures as function of uptake interval and lesion selection in non-small cell lung cancer patients. *J Nucl Med*. 2016;57:1343–1349.
15. Weber WA, Gatsonis CA, Mozley PD, et al. Repeatability of 18F-FDG PET/CT in Advanced non-small cell lung cancer: prospective assessment in 2 multicenter trials. *J Nucl Med*. 2015;56:1137–1143.
16. Velasquez LM, Boellaard R, Kollia G, et al. Repeatability of 18F-FDG PET in a multicenter phase I study of patients with advanced gastrointestinal malignancies. *J Nucl Med*. 2009;50:1646–1654.
17. Doot RK, Scheuermann JS, Christian PE, Karp JS, Kinahan PE. Instrumentation factors affecting variance and bias of quantifying tracer uptake with PET/CT. *Med Phys*. 2010;37:6035–6046.
18. Boellaard R, O’Doherty MJ, Weber WA, et al. FDG PET and PET/CT: EANM procedure guidelines for tumour PET imaging: version 1.0. *Eur J Nucl Med Mol Imaging*. 2010;37:181–200.
19. Lodge MA, Chaudhry MA, Wahl RL. Noise considerations for PET quantification using maximum and peak standardized uptake value. *J Nucl Med*. 2012;53:1041–1047.
20. Akamatsu G, Ikari Y, Nishida H, et al. Influence of statistical fluctuation on reproducibility and accuracy of SUV_{max} and SUV_{peak}: a phantom study. *J Nucl Med Technol*. 2015;43:222–226.
21. Makris NE, Huisman MC, Kinahan PE, Lammertsma AA, Boellaard R. Evaluation of strategies towards harmonization of FDG PET/CT studies in multicentre trials: comparison of scanner validation phantoms and data analysis procedures. *Eur J Nucl Med Mol Imaging*. 2013;40:1507–1515.
22. Armstrong IS, Kelly MD, Williams HA, Matthews JC. Impact of point spread function modelling and time of flight on FDG uptake measurements in lung lesions using alternative filtering strategies. *EJNMMI Phys*. 2014;1:99.
23. Shao X, Shao X, Wang X, Wang Y. Applications of both time of flight and point spread function in brain PET image reconstruction. *Nucl Med Commun*. 2016;37:422–427.
24. Rahmim A, Qi J, Sossi V. Resolution modeling in PET imaging: theory, practice, benefits, and pitfalls. *Med Phys*. 2013;40:064301-1–064301-15.
25. Boellaard R. Standards for PET image acquisition and quantitative data analysis. *J Nucl Med*. 2009;50:11S–20S.

SUPPORTING INFORMATION

Additional Supporting Information may be found online in the supporting information tab for this article.

Fig. S1. RC of NEMA IQ phantom data as a function of sphere diameter. Data acquired on the Philips Ingenuity system and based on images with a $4 \times 4 \times 4 \text{ mm}^3$ voxel size and 2-min starting frame duration using TOF on the left column and TOF + PSF on the right column. Figures (A and B) represent RC (%) for max, (C and D), peak, and (E and F) mean SUVs. Dotted lines correspond to the true RC based on the true activity within the phantom spheres. Boxes represent standard deviation (SD), whiskers show ranges, and solid line depicts median of the data.

Fig. S2. RC of NEMA IQ phantom data as a function of sphere diameter. Data acquired on the Siemens Biograph system and based on images with a $3.1819 \times 3.1819 \times 2 \text{ mm}$ voxel size and 2-min starting frame duration using TOF on the left column and TOF + PSF on the right column. Figures (A and B) represent RC (%) for max, (C and D), peak and (E and F) mean SUVs. Dotted lines correspond to the true RC based on the true activity within the phantom spheres. Boxes represent standard deviation (SD), whiskers show ranges, and solid line depicts median of the data.

Fig. S3. Maximum RC (%) of NEMA IQ phantom data as a function of sphere diameter. Data acquired on the Philips Ingenuity system and based on images with a $2 \times 2 \times 2 \text{ mm}^3$ voxel size and 2-min starting frame duration using TOF on the left and TOF + PSF on the right. Dotted lines correspond to the true RC based on the true activity within the phantom spheres. Boxes represent standard deviation (SD), whiskers show ranges, and solid line depicts median of the data.

Fig. S4. Maximum RC (%) of NEMA IQ phantom data as a function of sphere diameter. Data acquired on the Siemens Biograph system and based on images with a $2 \times 2 \times 2 \text{ mm}^3$ voxel size and 2-min starting frame duration using TOF on the left and TOF + PSF on the right. Dotted lines correspond to the true RC based on the true activity within the phantom spheres. Boxes represent standard deviation (SD), whiskers show ranges, and solid line depicts median of the data.